Interfaces and multicomponent fluids

Junseok Kim and John Lowengrub
Department of Mathematics
University of California, Irvine, USA
E-mail: lowengrb@math.uci.edu

December 28, 2004

1   Introduction

Many important industrial problems involve flows with multiple constitutive components. Examples include extractors, separators, reactors, sprays, polymer blends, and microfluidic applications such as DNA analysis, and protein crystallization. Due to inherent nonlinearities, topological changes, and the complexity of dealing with unknown, active, and moving surfaces, multiphase flows are challenging. Much effort has been put into studying such flows through analysis, asymptotics, and numerical simulation. Here, we focus on review on studies of multicomponent fluids using continuum numerical methods.

There are many ways to characterize moving interfaces. The two main approaches to simulating multiphase and multicomponent flows are interface tracking and interface capturing. In interface tracking methods (examples include boundary integral methods, volume-of-fluid, front-tracking, immersed boundary, and immersed interface), Lagrangian (or semi-Lagrangian) particles are used to track the interfaces. In boundary-integral methods, the flow equations are mapped from the immiscible fluid domains to the sharp interfaces separating them thus reducing the dimensionality of the problem (the computational mesh discretizes only the interface). In interface capturing methods such as level-set and phase-field methods, the interface is implicitly

captured by a contour of a particular scalar function.

The equations governing the motion of an unsteady, viscous, incompressible, immiscible two-fluid system are the Navier-Stokes equations (the subscript i denotes the ith flow component):

$$\rho_i \left(\frac{\partial \mathbf{u}_i}{\partial t} + \mathbf{u}_i \cdot \nabla \mathbf{u}_i \right) = \nabla \cdot \sigma_i + \rho_i \mathbf{g}, \quad i = 1, 2, \tag{1}$$

$$\sigma_i = -p_i \mathbf{I} + 2\eta_i \mathbf{D}_i \tag{2}$$

where ρ_i is the density, $\mathbf{u}_i$ is the fluid velocity, p_i is the pressure, η_i is the viscosity, and $\mathbf{g}$ is the gravitational acceleration vector. In Eq. (2), σ_i is the stress tensor, $\mathbf{I}$ is the identity matrix, and $\mathbf{D}_i$ is the rate of deformation tensor and defined as $\mathbf{D}_i = \frac{1}{2}(\nabla \mathbf{u}_i + \nabla \mathbf{u}_i^T)$. The velocity field is subject to the incompressibility constraint,

$$\nabla \cdot \mathbf{u}_i = 0. \tag{3}$$

We let Γ denote the fluid interface. The effect of surface tension is to balance the jump of the normal stress along the fluid interface. This gives rise to a Laplace-Young condition for the discontinuity of the normal stress across Γ:

$$[\sigma \mathbf{n}]_\Gamma = \tau \kappa \mathbf{n}, \tag{4}$$

where $[\sigma]_\Gamma$ denotes the jump $\sigma_2 - \sigma_1$ across Γ, κ is the curvature of Γ (positive for a spherical interface), τ is the surface tension coefficient which is assumed to be constant, and $\mathbf{n}$ is the unit normal vector along Γ directed toward fluid 2. The fluid velocity is continuous across Γ.

In order to circumvent the problems associated with implementing the Laplace-Young calculation at the exact interface boundary, Brackbill et al. [5] developed a method referred to as the continuum surface force (CSF) method. In this method, the surface tension jump condition is converted into an equivalent singular volume force that is added to the Navier-Stokes equations. Typically, the singular force is smoothed and acts only in a finite transition region across the interface. The system of equations (1)-(2) and the boundary condition, Eq. (4) can be combined into the following distribution formulation that holds in both phases:

$$\rho \left(\mathbf{u}_t + \mathbf{u} \cdot \nabla \mathbf{u} \right) = -\nabla p + \nabla \cdot (2\eta \mathbf{D}) + \rho \mathbf{g} + \mathbf{F}_{sing}, \quad \nabla \cdot \mathbf{u} = 0 \tag{5}$$

where the subscript i is dropped (i.e. it is understood that $\mathbf{u} = \mathbf{u}_i$ in fluid i, etc.) and $\mathbf{F}_{sing}$ is singular surface tension force that is given by $\mathbf{F}_{sing} = -\tau\kappa\delta_\Gamma\mathbf{n}$, where δ_Γ is the surface delta function.

2 Numerical methods for multicomponent fluid flows

2.1 Interface tracking methods

2.1.1 Boundary integral methods

Boundary integral methods (BIM) can be highly accurate for modeling free surface flows with relatively regular interface topologies. The BIM was apparently first used by Rosenhead [39] to study vortex sheet roll-up. In this approach, the interface is explicitly tracked, but the flow solution in the entire domain is deduced solely from information possessed by discrete points along the interface.

Boundary integral methods have been used for both inviscid and Stokes flows. For a review of Stokes flow computations, see Pozrikidis [36], and for a review of computations of inviscid flows, see Hou et al. [17]. For flows with both inertia and viscosity, volume integrals must be incorporated into the formulation.

When inertial forces are negligible (left hand side term of Eq. (1) is dropped), the velocity $\mathbf{u}(\mathbf{x}_0)$ at a given point $\mathbf{x}_0$ on the interface can be obtained by means of the boundary integral formulation,

$$(\lambda + 1)\mathbf{u}(\mathbf{x}_0) = 2\mathbf{u}_\infty(\mathbf{x}_0) - \frac{1}{4\pi}\int_\Gamma f(\mathbf{x})\mathbf{G}(\mathbf{x}_0, \mathbf{x}) \cdot \mathbf{n}(\mathbf{x})ds(\mathbf{x}) \qquad (6)$$

$$-\frac{\lambda - 1}{4\pi}\int_\Gamma \mathbf{u}(\mathbf{x}) \cdot \mathbf{T}(\mathbf{x}_0, \mathbf{x}) \cdot \mathbf{n}(\mathbf{x})ds(\mathbf{x}), \qquad (7)$$

where λ is the viscosity ratio, $\mathbf{u}_\infty$ is an imposed velocity prevailing in the absence of the interfaces, and $f(\mathbf{x})$ is the capillary force function $f = \tau\kappa$.

The tensors $\mathbf{G}$ and $\mathbf{T}$ are the Stokeslet and stresslet, respectively,

$$\mathbf{G}(\mathbf{x}_0, \mathbf{x}) = \frac{\mathbf{I}}{r} + \frac{\hat{\mathbf{x}}\hat{\mathbf{x}}}{r^3}, \quad \mathbf{T}(\mathbf{x}_0, \mathbf{x}) = -\frac{6\hat{\mathbf{x}}\hat{\mathbf{x}}\hat{\mathbf{x}}}{r^5}, \tag{8}$$

$$\text{where } \hat{\mathbf{x}} = \mathbf{x} - \mathbf{x}_0, \ r = |\hat{\mathbf{x}}|. \tag{9}$$

The boundary conditions at the interface, i.e. the stress balance equation (4) and continuity of the velocity across the interface, are automatically satisfied by the boundary integral formulation.

The normal velocity of the interface $\Gamma(\mathbf{x}, t)$ is given by

$$\frac{d\mathbf{x}}{dt} \cdot \mathbf{n}(\mathbf{x}) = \mathbf{u}(\mathbf{x}, \mathbf{t}) \cdot \mathbf{n}(\mathbf{x}). \tag{10}$$

The shape of the interface does not depend on the tangential velocity and there are many possible choices that can be taken, see Hou et al. [17].

The principal advantages gained by using boundary integral methods are the reduction of the flow problem by one dimension since the formulation involves quantities defined on the interface only and the potential for highly accurate solutions if the flow has topologically regular interfaces. In addition, highly efficient adaptive surface mesh refinement algorithms have recently been developed to the improve performance and accuracy of the methods [9]. The main disadvantages are the development of accurate quadratures of integrals with singular kernels (particularly in 3D) and the need for local surgery of the interface in the event of topological changes.

Boundary integral methods have been successfully used for simulations of complex multiphase flows: drop deformation and breakup; jets; capillary waves; mixing; drop-to-drop interaction; suspension of liquid drops in viscous flow (e.g. see [4, 9, 17, 36] and the references therein).

2.1.2 Volume-of-fluid method

The VOF method was first reported in Nichols and Hirt [30], and more completely in Hirt and Nichols [18]. In the VOF method (see Scardovelli and Zaleski [51] for a recent review), the location of the interface is determined by the volume fraction c_{ij} of fluid 1 in the computational cell, Ω_{ij}. In cells containing the interface $0 < c_{ij} < 1$, $c_{ij} = 1$ in cells containing fluid 1, and $c_{ij} = 0$ in cells containing fluid 2 as shown in Fig. 1(b).

A VOF algorithm is divided into two parts: a reconstruction step and a propagation step. A typical interface reconstruction is shown in Fig. 1(c). In the piecewise linear interface construction (PLIC) method, the true interface as shown in Fig. 1(a), is approximated by a straight line perpendicular to an interface normal vector $\mathbf{n}_{ij}$ in each cell Ω_{ij}. The normal vector $\mathbf{n}_{ij}$ is determined from the volume fraction gradient using data from neighboring cells. With given a volume fraction c_{ij} and a normal vector $\mathbf{n}_{ij}$, the interface is given by the straight line with normal $\mathbf{n}_{ij}$ such that area beneath the line in cell Ω_{ij} is equal to c_{ij}. In [42], a parabolic reconstruction (PROST) of the interface is used to gain higher order accuracy for the surface tension force.

Once the interface has been reconstructed, its motion by the underlying flow field must be modeled by a suitable advection algorithm. The key here is that the explicit interface reconstruction enables fluxes to be developed that exactly conserve mass and do not diffuse the interface.

Capillary effects may be represented by the continuous surface stress [51],

$$\mathbf{T} = -\tau(\mathbf{I} - \mathbf{n} \otimes \mathbf{n})|\nabla \tilde{c}|, \ \mathbf{F}_{sing} = -\nabla \cdot \mathbf{T}, \tag{11}$$

where $\tilde{c}$ is a smoothed version of the volume fraction. For the flows in which the capillary force is the dominant physical mechanism, the PROST algorithm discussed above can be used to significantly reduce spurious currents due to inaccurate representation of surface tension terms and associated pressure jump in normal stress.

The distribution form of the fluid equations (5) is typically solved using a variant of the projection method (e.g. see [37]) originally developed by Chorin [8] for single phase flows.

VOF methods are popular and have been used in commercial multiphase flow codes, in models of ink-jet printers [55], flows with surfactants [43, 10, 14] and in many other applications (e.g. see [51] and the references therein). The principal advantage of VOF methods is their inherent volume conserving property. Nevertheless, spurious bubbles and drops may be created. The reconstruction of the interface from the volume fractions and the computation of geometric quantities such as curvature are typically less accurate than other methods discussed here since the curvature and normal vectors are obtained by differentiating a nearly discontinuous function (volume fraction).

2.1.3   Front-tracking methods

The basic idea behind the original front tracking method is the use of two grids as illustrated in Fig. 2. One is a standard, Eulerian finite difference mesh that is used to solve the fluid equations. The other is a discretized interface mesh that is used to explicitly track the interface and compute surface tension force which is then transferred to the finite difference mesh via a discrete delta-function. Front tracking was first proposed by Richtmyer and Morton [41] and further developed by Glimm et al. [15].

A similar approach was taken by Unverdi and Tryggvason (see [52] and [34] for recent reviews), who combined a moving grid description of the interface with flow computations on a fixed grid. In this immersed boundary approach, all the fluid phases are treated together by solving a single set of governing equations. This method has its roots in the original marker-and-cell (MAC) method [19], where marker particles are used to identify each fluid and the immersed boundary method of Peskin and McQueen [35], that was designed to track moving elastic boundaries in homogeneous fluids.

The interface is represented discretely by Lagrangian markers that are connected to form a front which lies within and moves through a stationary Eulerian mesh.

In Tryggvason's original implementation, the basic structural unit is a line segment. Since the interface moves and deforms during the computation, interface elements must occasionally be added or deleted to maintain regularity and stability. In the event of merging/breakup, elements must be relinked to effect a change in topology.

The interface is represented using an ordered list of marker particles $\mathbf{x}_k = ((x_1)_k, (x_2)_k)$, $1 \leq k \leq N$. The first step in this algorithm is the advection of the marker particles. A simple bilinear interpolation is used to find the velocity inside each grid cell (indicated in Fig. 2(c)). The marker particles are then advected in a Lagrangian manner. Once the points have been advected, a list of connected polynomials $(p_i^x(s), p_i^y(s))$ is constructed using the marker particles. This gives a parametric representation of the interface, with s typically an approximation of the arc length. Both lists are ordered and thus identify the topology of the interface. In later works, higher order polynomials have been used (e.g. cubic splines) and semi-Lagrangian evolutions have been implemented where other tangential velocities have been

used [6].

As the interface evolves, the markers drift along the interface following tangential velocities and more markers may be needed if the interface is stretched by the flow. Typically, the markers are redistributed along the interface to maintain an accurate interface representation.

Next, we compute the surface tension force,

$$\mathbf{F}_{sing}(\mathbf{x}, t) = \int_{\Gamma(t)} \tau \kappa_f \delta(\mathbf{x} - \mathbf{x}_f(s)) \mathbf{n}_f ds, \tag{12}$$

where the subscript f means values evaluated at the interface, $\Gamma(t)$ and s is arclength. The discrete numerical implementation of this distribution onto the fixed grid is (following [47]) in the form of a sum over interface elements, $\mathbf{x}_{f,k}$:

$$\mathbf{F}_{ij}(\mathbf{x}) = \sum_k \mathbf{f}_k \delta(\mathbf{x} - \mathbf{x}_{f,k}) \Delta s_k, \tag{13}$$

where Δs_k is the average of the straight line distances from the point $\mathbf{x}_{f,k}$ to the two neighboring points $\mathbf{x}_{f,k+1}$ and $\mathbf{x}_{f,k-1}$ as indicated by the sub-grid control volume shown in figures 2(a) and (b). The delta function is typically taken to be Peskin's discrete Dirac delta function [35]:

$$\delta(\mathbf{x} - \mathbf{x}_{f,k}) = \begin{cases} \prod_{i=1}^{2} \frac{1}{4h} \left(1 + \cos \frac{\pi [\mathbf{x}_i - (\mathbf{x}_{f,i})_k]}{2h}\right) & \text{if } |\mathbf{x} - \mathbf{x}_{f,k}| \leq 2h \\ 0 & \text{otherwise} \end{cases} \tag{14}$$

Another higher order alternative form of the regularized delta function using the product formula is found in [53].

Using the Frenet relation, the surface tension force on a short segment of the front is given by

$$\mathbf{f}_k = \int_A^B \tau \kappa_f \mathbf{n}_f ds = \int_A^B \tau \frac{\partial \mathbf{t}_f}{\partial s} ds = \tau(\mathbf{t}_B - \mathbf{t}_A), \tag{15}$$

where A and B are the segment endpoints that lie on the boundary of the subgrid control volume (Figs. 2(a) and (b)), and $\mathbf{t}_f$ is a tangent vector computed by fitting a polynomial to the end points of each element.

In the case of flows with varying density and/or viscosity between the fluid components, there is a need to calculate the phase indicator function $I(\mathbf{x}, t)$ (defined by interface geometry and position), which has the value 0 in fluid 1 and 1 in fluid 2. The indication function can be determined via the solution of the equation

$$\Delta I(\mathbf{x}, t) = \nabla \cdot \int_{\Gamma(t)} \mathbf{n}_f \delta(\mathbf{x} - \mathbf{x}_f(s, t)) ds. \tag{16}$$

This equation is discretized on the Eulerian mesh and a discrete delta-function (e.g. Eq. (14)) is used. The fluid properties such as density and viscosity are determined via the indicator function, i.e. $\rho(\mathbf{x}, t) = \rho_1 + (\rho_2 - \rho_1) I(\mathbf{x}, t)$, etc.

As in the volume of fluid algorithm, the distribution form of the Navier-Stokes equations (5) are typically solved using a version of Chorin's projection method.

An alternative flow solver that can be used to integrate the flow equations in the presence of an interface is the immersed interface method. The immersed interface method (IIM) was developed in [26], extended in [27], and can be used together with front-tracking (as well as level-set [13]) methods.

The IIM directly incorporates jump conditions for the normal stress into the finite difference stencil. The key idea of this method is to use the jump conditions in Taylor series expansions of pressure and velocity near interfaces to derive difference equations that achieve pointwise second-order accuracy.

The principal advantage of front-tracking algorithms is their inherent accuracy, due in part to the ability to use a large number of grid points on the interface. Front-tracking methods can be complicated to implement, particularly in 3D, but give the precise location and geometry of the interface. In addition, explicit front tracking permits more than one interface to be present in a single computational cell without coalescence, which can be important in dense bubbly flows, emulsions, etc. One of major handicaps of front tracking methods is the difficulty in modeling topological changes of the interface such as break-up and coalescence without ad-hoc cut-and-connect and reconnecting parameterized interface (particularly, difficulties in 3D).

2.2 Interface capturing methods

2.2.1 Level set method

Level set methods, introduced by Osher and Sethian [33] (see the recent review papers [31, 50] and the recent texts [32, 44]), are popular computational techniques for tracking moving interfaces. These methods rely on an implicit representation of the interface as the zero set of an auxiliary function (level-set function). The application of these methods to incompressible, multiphase flows started with the work of Sussman et al. [49] and Chang et al. [7].

In the level set method, the level set function $\phi(\mathbf{x}, t)$ is defined as follows (see Fig. 3):

$$\phi(\mathbf{x}, t) \begin{cases} > 0, & \text{if } \mathbf{x} \in \text{fluid 1} \\ = 0, & \text{if } \mathbf{x} \in \Gamma \text{ (the interface between fluids)} \\ < 0, & \text{if } \mathbf{x} \in \text{fluid 2} \end{cases}$$

and the evolution of ϕ is given by

$$\phi_t + \mathbf{u} \cdot \nabla\phi = 0, \tag{17}$$

which means that the interface moves with fluid.

To keep the interface geometry well resolved, the level-set function ϕ should be a distance function near the interface. However, under the evolution (17) it will not necessarily remain as such. We note that special velocity extensions $\mathbf{v}$ off the interface (i.e. $\mathbf{v} = \mathbf{u}$ at the interface, $\mathbf{v} \neq \mathbf{u}$ away from interface) have been recently developed to better maintain ϕ as a distance function (e.g. [3, 29]). Typically, a reinitialization step (solving a Hamilton-Jacobi type equation, Eq. (18)) below, is performed to keep ϕ as a distance function near the interface while keeping original zero level set unchanged. More specifically, given a level set function, ϕ, at time t, the contours are redistributed according to the steady state solution of the equation

$$\frac{\partial d}{\partial \tau} = S_\epsilon(\phi)(1 - |\nabla d|), \quad d(\mathbf{x}, 0) = \phi(\mathbf{x}), \tag{18}$$

where S_ϵ is the smoothed sign function defined as

$$S_\epsilon(\phi) = \frac{\phi}{\sqrt{\phi^2 + \epsilon^2}}, \tag{19}$$

where ϵ is usually is one or two grid lengths. After solving Eq. (18) to steady state $\phi(\mathbf{x}, t)$ is then replaced by $d(\mathbf{x}, \tau_{steady})$. Note that $d(\mathbf{x}, \tau_{steady})$ is typically a good approximation of the signed distance function.

The density and viscosity are defined as

$$\rho(\phi) = \rho_2 + (\rho_1 - \rho_2)H_\epsilon(\phi) \text{ and } \eta(\phi) = \eta_2 + (\eta_1 - \eta_2)H_\epsilon(\phi), \tag{20}$$

where $H_\epsilon(\phi)$ is the smoothed Heaviside function given by

$$H_\epsilon(\phi) = \begin{cases} 0 & \text{if } \phi < -\epsilon \\ \frac{1}{2}\left[1 + \frac{\phi}{\epsilon} + \frac{1}{\pi}\sin(\pi\phi/\epsilon)\right] & \text{if } |\phi| \leq \epsilon \\ 1 & \text{if } \phi > \epsilon. \end{cases}$$

The mollified delta function is $\delta_\epsilon(\phi) = dH_\epsilon/d\phi$. The surface tension force is given as

$$\mathbf{F}_{sing} = -\tau \nabla \cdot \left(\frac{\nabla\phi}{|\nabla\phi|}\right) \delta_\epsilon(\phi) \frac{\nabla\phi}{|\nabla\phi|}. \tag{21}$$

The fluid equations (5) are solved using projection methods, the IIM or the ghost-fluid (GF) method (e.g. [12]). The GF method is similar to the IIM in that jump discontinuities are incorporated in the finite difference stencil. In the GF algorithm, subcell resolution is used to mark the interface position and the values of discontinuous quantities are artificially extended to grid points neighboring the interface via extrapolation. A fully second order accurate GF method for moving interfaces has recently been developed [29].

Applications of the level-set method include multiphase flows, viscoelastic fluid flows and fluid-structure interactions (e.g. see the reviews [31, 50, 32, 44]).

Advantages of the level-set algorithm include the simplicity with which it can be implemented, the ability to capture merging and beak up of interfaces automatically, and the ease with which the interface geometry can be described

using the level set function. A disadvantage of the level set method is that mass is not conserved.

Accurate numerical simulations of multiphase flow and topology transitions require the computational mesh to resolve both the macro scales (e.g. droplet size, flow geometry) and the micro scales to accurately capture local interface geometries near contact region, van der Waals forces, surfactant distribution, and Marangoni stresses. Adaptive mesh algorithms have recently been used greatly increase accuracy and computational efficiency in level-set methods [45]. For example, in [45], a Cartesian adaptive level-set is used to solve the incompressible Navier-Stokes equations with a free boundary. This method has been used to simulate droplet formation in inkjet printers and to compute the wake of a ship. Another approach, recently developed, is to use adaptive unstructured mesh refinement [56], as shown in Fig. 4, in which the impact of a drop onto a fluid interface is captured.

2.3 Hybrid methods

More recently, a number of hybrid methods, which combine good features of each algorithm, have been developed. These include coupled level-set volume-of-fluid (CLSVOF) algorithms, particle level-set methods, marker-VOF methods and level-contour front tracking methods.

Level set and volume-of-fluid methods have been combined in [48, 46]. The volume fraction is used to maintain volume conservation, while the level-set function is used to describe the interface geometry. After every time step, the volume fraction function and level-set function are made compatible. The coupling between the level set function ϕ and the volume-of-fluid function c occurs through the normal of the reconstructed interface and through the fact that the level set function is reset to the exact signed normal distance to the reconstructed interface (where the area below the reconstructed interface is given by the volume fraction function).

In the particle level-set method [11], Lagrangian disconnected marker particles are randomly positioned near the interface and are passively advected by the flow in order to rebuild the level set function in underresolved zones, such as high curvature regions and near filaments. In these regions, the standard non-adaptive level-set method regularizes excessively the interface structure and mass is lost. The use of marker particles significantly ameliorates these

difficulties.

In [1], a hybrid method is developed, which uses both marker particles, to reconstruct and move the interface, and the volume fraction function to conserve volume. In this approach, a smooth motion of the interface, typical of marker methods is obtained together with volume conservation, as in standard VOF methods. This work improves both the accuracy of interface tracking, when compared to standard VOF methods, and the conservation of mass, with respect to the original marker method.

In [47], a hybrid method that combines a level contour reconstruction technique with front tracking methods has recently been developed to automatically model the merging and breakup of interfaces in three-dimensional flows.

2.4   Phase-field method

Phase field, or diffuse-interface, models are an increasingly popular choice for modeling the motion of multiphase fluids (see [2] for a recent review). In the phase-field model, sharp fluid interfaces are replaced by thin but nonzero thickness transition regions where the interfacial forces are smoothly distributed. The basic idea is to introduce a conserved order parameter (e.g., mass concentration) that varies continuously over thin interfacial layers and is mostly uniform in the bulk phases (see Fig. 5).

For density-matched binary liquids (let $\rho = 1$ for simplicity), the coupling of the convective Cahn-Hilliard equation for the mass concentration with a modified momentum equation that includes a phase field-dependent surface force is known as Model H [16]. In the case of fluids with different densities a phase field model has been proposed by Lowengrub and Truskinovsky [28]. Complex flow morphologies and topological transitions such as coalescence and interface break-up can be captured naturally and in a mass-conservative and energy-dissipative fashion since there is an associated free energy functional.

The phase field is governed by the following advective Cahn-Hilliard equation:

$$\frac{\partial c}{\partial t} + \mathbf{u} \cdot \nabla c = \nabla \cdot (M(c)\nabla\mu), \tag{22}$$

$$\mu = F'(c) - \epsilon^2 \Delta c, \tag{23}$$

where $M(c) = c(1-c)$ is the mobility, $F(c) = \frac{1}{4}c^2(1-c)^2$ is a Helmholtz free energy that describe the coexistence of immiscible phases, and ϵ is a measure of interface thickness and $\epsilon \sim \xi$ (see Fig. 5). It can be shown that in the sharp interface limit $\epsilon \to 0$, the classical Navier-Stokes system equations and jump conditions are recovered [28].

The singular surface tension force is $\mathbf{F}_{sing} = -6\sqrt{2}\tau\epsilon\nabla \cdot (\nabla c \otimes \nabla c)$, where τ is the surface tension coefficient [28]. An alternative surface tension force formulation based on the CSF is $\mathbf{F}_{sing} = -6\sqrt{2}\tau\epsilon\nabla \cdot (\frac{\nabla c}{|\nabla c|})|\nabla c|\nabla c$, see [22].

Recently, very efficient nonlinear multigrid methods have been developed to solve implicit discretizations of the Cahn-Hilliard equation [23, 24]. These schemes have been combined with projection methods to solve the Navier-Stokes equations to perform simulations of multiphase flows (e.g. see [23, 21]). Alternative numerical approaches can be found in [57] and [20].

An example of simulation of liquid thread breakup using a phase-field method is shown in Fig. 6 (adapted from [21]). A long cylindrical thread of a viscous fluid 1 is in an infinite mass of another viscous fluid 2. If the thread becomes varicose with wave-length λ, the equilibrium of the column is unstable, provided λ exceeds the circumference of the cylinder. This is the Rayleigh capillary instability [40] that results in surface-tension driven breakup of the thread.

An advantage of the phase field approach is that it is straightforward to include more complex physical effects. For example, the binary model can be straightforwardly extended to describe three component flows as follows. Consider a ternary mixture and denote the composition of components 1, 2, and 3, expressed as mass fractions, by c_1, c_2, and c_3, respectively. Therefore,

$$\sum_{i=1}^{3} c_i = 1, \quad 0 \leq c_i \leq 1. \tag{24}$$

The composition of a ternary mixture (A, B, and C) can be mapped onto an equilateral triangle (the Gibbs triangle [38]) whose corners represent 100% concentration of A, B or C as shown in Fig. 7(a). Mixtures with components lying on lines parallel to $\overline{BC}$ contain the same percentage of A, those with lines parallel to $\overline{AC}$ have the same percentage of B concentration, and analogously for the C concentration. In Fig. 7(a), the mixture at the position marked 'o' contains 60% A, 10% B, and 30% C. Because the concentrations

sum to unity, only two of them need to be determined, say c_1, c_2.

The evolution of c_1 and c_2 is governed by the following advective ternary Cahn-Hilliard equation:

$$\frac{\partial c_1}{\partial t} + \mathbf{u} \cdot \nabla c_1 = \nabla \cdot (M(c_1, c_2) \nabla \mu_1), \tag{25}$$

$$\frac{\partial c_2}{\partial t} + \mathbf{u} \cdot \nabla c_2 = \nabla \cdot (M(c_1, c_2) \nabla \mu_2), \tag{26}$$

$$\mu_1 = \frac{\partial F(c_1, c_2)}{\partial c_1} - \epsilon^2 \Delta c_1 - 0.5\epsilon^2 \Delta c_2, \tag{27}$$

$$\mu_2 = \frac{\partial F(c_1, c_2)}{\partial c_2} - 0.5\epsilon^2 \Delta c_1 - \epsilon^2 \Delta c_2, \tag{28}$$

where $M(c_1, c_2) = \sum_{i<j}^3 c_i c_j$ is the mobility and $F(c_1, c_2)$ is the Helmholtz free energy that can be used to model the miscibility of the components. An example of a free energy (used in the simulation shown in figure 8 below) for which fluids 1 and 3 are immiscible and fluid 2 is preferentially miscible with fluid 3 is:

$$F(c_1, c_2) = 2c_1^2 \left(1 - c_1 - c_2\right)^2 + (c_1 + 0.2)\left(c_2 - 0.2\right)^2 + (1.2 - c_1 - c_2)\left(c_2 - 0.4\right)^2.$$

The contours of F on the Gibbs triangle are shown in figure 7(b).

The singular surface tension force is $\mathbf{F}_{sing} = -6\sqrt{2}\epsilon \sum_{i=1}^3 \tau_i \nabla \cdot (\nabla c_i \otimes \nabla c_i)$, where the physical surface tension coefficients τ_{ij} between two fluids i and j are decomposed into the phase specific surface tensions τ_i such that $\tau_{ij} = \tau_i + \tau_j$.

As a demonstration of the evolution possible in partially miscible liquid systems, we present an example in which there is a gravity-driven (Rayleigh-Taylor) instability that enhances the transfer of a preferentially miscible contaminant from one immiscible fluid to another in 2D. In this system, the ternary Cahn-Hilliard system is solved using nonlinear multigrid methods and a projection method [25] is used to solve the flow equations (5).

In Fig. 8 (first column), the top half of the domain initially consists of a mixture of fluids 1 and 2, and the bottom half consists of fluid 3, which is immiscible with fluid 1. The contours of c_1, c_2, and c_3 are visualized in grayscale where darker regions denote larger values of c_1, c_2, and c_3, respectively. In the top row, the contours of fluid 1 are shown, the middle and bottom rows correspond to fluids 2 and 3 respectively.

Fluid 2 is preferentially miscible with fluid 3. Fluid 1 is assumed to be the lightest and fluid 2 the heaviest. The density of the 1/2 mixture is heavier than that of fluid 3, so the density gradient induces the Rayleigh-Taylor Instability.

The evolution of the three phases is shown in Fig. 8. As the simulation begins, the 1/2 mixture falls and fluid 2 diffuses into fluid 3. A characteristic Rayleigh-Taylor (inverted) mushroom forms, the surface area of the 1/3 interface increases, and vorticity is generated and shed into the bulk. As fluid 2 is diffused from fluid 1, the pure fluid 1 rises to the top as shown in Fig. 8. Imagining that fluid 2 is a contaminant in fluid 1, this configuration provides an efficient means of cleansing fluid 1 since the buoyancy-driven flow enhances the diffusional transfer of fluid 2 from fluid 1 to fluid 3.

The advantages of the phase-field method are: (1) topology changes are automatically described; (2) the composition field c has a physical meaning not only on near interface but also in the bulk phases; (3) complex physics can easily be incorporated into the framework, the methods can be straightforwardly extended to multicomponent systems, and miscible, immiscible, partially miscible, and lamellar phases can be modeled.

Associated with diffuse-interfaces is a small scale ϵ, proportional to the width of the interface. In real physical systems describing immiscible fluids, ϵ can be vanishingly small. However, for numerical accuracy ϵ must be at least a few grid lengths in size. This can make computations expensive. One way of ameliorating this problem is to adaptively refine the grid only near the transition layer. Such methods are under development by various research groups.

Phase-field methods have been used to model viscoelastic flow, thermocapillary flow, spinodal decomposition, the mixing and interfacial stretching, in a shear flow, droplet breakup process, wave-breaking and sloshing, the fluid motion near a moving contact line, and the nucleation and annihilation of an equilibrium droplet (see the references in the review paper [2]).

3 Conclusions and future directions

In this paper we have reviewed the basic ideas of interface tracking and interface capturing methods that are critical in simulating the motion of inter-

faces in multicomponent fluid flows. The differences between these various formulations lie in the representation and the reconstruction of interfaces. The advantages and disadvantages of the algorithms have been discussed. While there has been much progress on the development of robust multi-fluid solvers, there is much more work to be done. Promising future directions for research include the incorporation of adaptive mesh refinement into the algorithms and the development of efficient hybrid schemes that combine the best features of individual methods.

See also

Capillary surfaces
Modeling fluid behaviors
Inviscid flows
Non-Newtonian fluids
Vortex dynamics
Waves in fluids
Incompressible Euler Equations: mathematical theory
Partial differential equations in fluid mechanics
Numerical methods in fluid mechanics
Viscous incompressible fluids: mathematical theory

Keywords

multiphase, surface tension, interface dynamics, interface tracking, interface capturing, volume-of-fluid, boundary integral, front-tracking, immersed boundary, immersed interface, level-set, phase-field

References

[1] E. Aulisa, S. Manservisi, and R. Scardovelli, A mixed markers and volume-of-fluid method for the reconstruction and advection of interfaces in two-phase and free-boundary flows, J. Comput. Phys. 188 (2003) 611-639

[2] D.M. Anderson, G.B. McFadden, and A.A. Wheeler, Diffuse-interface methods in fluid mechanics, Ann. Rev. Fluid Mech. 30 (1998) 139-165.

[3] D. Adalsteinsson and J.A. Sethian, The fast construction of extension velocities in level set methods, J. Comput. Phys. 148 (1999) 2-22.

[4] I.B. Bazhlekov, P.D. Anderson, and H.E.H. Meijer, Nonsingular boundary integral method for deformable drops in viscous flows, Phys. Fluids 16 (2004) 1064-1081.

[5] J.U. Brackbill, D.B. Kothe, and C. Zemach, A continuum method for modeling surface tension, J. Comput. Phys. 100 (1992) 335-354.

[6] H.D. Ceniceros and A.M. Roma, Study of the long-time dynamics of a viscous vortex sheet with a fully adaptive nonstiff method, Phys. Fluids 16 (2004) 4285-4318.

[7] Y.C. Chang, T.Y. Hou, B. Merriman and S. Osher, A level set formulation of Eulerian interface capturing methods for incompressible fluid flows. J. Comp. Phys. 124 (1996) 449-464.

[8] J. Chorin, Numerical solution of the NavierStokes equations, Math. Comput. 22 (1968) 745-762.

[9] V. Cristini, J. Blawzdziewicz, and M. Loewenberg, An Adaptive Mesh Algorithm for Evolving Surfaces: Simulations of Drop Breakup and Coalescence J. Comput. Phys. 168 (2001) 445-463.

[10] M.A. Drumwright-Clarke and Y. Renardy, The effect of insoluble surfactant at dilute concentration on drop breakup under shear with inertia, Phys. Fluids 16 (2004) 14-21.

[11] D. Enright, R. Fedkiw, J. Ferziger, and I. Mitchell, A hybrid particle level set method for improved interface capturing, J. Comput. Phys. 183 (2002) 83-116.

[12] R.P. Fedkiw, T. Aslam, B. Merriman and S. Osher, A nonoscillatory approach to interfaces in multimaterial flows. J. Comp. Phys. 152 (1999) 457-492.

[13] T.Y. Hou, Z.L. Li, S. Osher and H.K. Zhao, A hybrid method for moving interface problems with application to the Hele-Shaw flow. J. Comp. Phys. 134 (1997) 236-252.

[14] A.J. James and J. Lowengrub, A surfactant-conserving volume-of-fluid method for interfacial flows with insoluble surfactant, J. Comput. Phys. 201 (2004) 685-722.

[15] J. Glimm, J.W. Grove, X.L. Li, K.-M. Shyue, Q. Zhang and Y. Zeng, Three-dimensional front tracking, SIAM J. Sci. Comput. 19 (1998) 703-727.

[16] P.C. Hohenberg, B.I. Halperin, Theory of dynamic critical phenomena, Rev. Mod. Phys. 49 (1977) 435-479.

[17] T.Y. Hou, J.S. Lowengrub, and M.J. Shelley, Boundary integral methods for multicomponent fluids and multiphase materials, J. Comput. Phys. 169 (2001) 302-362.

[18] C.W. Hirt and B.D. Nichols, Volume of Fluid (VOF) Method for the Dynamics of Free Boundaries, J. Comput. Phys. 39 (1981) 201-225.

[19] F.H. Harlow and J.E. Welch, The MAC method: a computing technique for solving viscous, incompressible, transient fluid flow problems involving free surface, Phys Fluids 8 (1965) 2182-2189

[20] D. Jacqmin, Calculation of two-phase Navier-Stokes flows using phase-field modeling, J. Comp. Phys. 155 (1999) 96-127.

[21] J.S. Kim, A diffuse-interface model for axisymmetric immiscible two-phase flow, Appl. Math. Comput. 160 (2005) 589-606.

[22] J.S. Kim, A continuous surface tension force formulation for diffuse-interface models, J. Comput. Phys. (2005), in press.

[23] J.S. Kim, K.K. Kang and J.S. Lowengrub, Conservative multigrid methods for Cahn-Hilliard fluids. J. Comp. Phys. 193 (2004) 511-543.

[24] J.S. Kim, K.K. Kang and J.S. Lowengrub, Conservative multigrid methods for ternary Cahn-Hilliard systems. Comm. Math. Sci. 2 (2004) 53-77.

[25] J.S. Kim and J.S. Lowengrub, Ternary Cahn-Hilliard fluids, under review.

[26] R. J. LeVeque and Z. Li, The immersed interface method for elliptic equations with discontinuous coeficients and singular sources, SIAM J. Numer. Anal. 31 (1994) 1019-1044.

[27] L. Lee and R.J. Leveque, An immersed interface method for incompressible Navier-Stokes equations, SIAM J. Sci. Comput. 25 (2003) 832-856.

[28] J.S. Lowengrub and L. Truskinovsky, Quasi-incompressible Cahn-Hilliard fluids and topological transitions, Proc. R. Soc. Lond. A 454 (1998) 2617-2654.

[29] P. Macklin and J.S. Lowengrub, Evolving interfaces via gradients of geometry-dependent interior Poisson problems: application to tumor growth, J. Comput. Phys. 203 (2005) 191-220.

[30] B.D. Nichols and C.W. Hirt, Methods for Calculating Multi-Dimensional, Transient Free Surface Flows Past Bodies, Proc. First Intern. Conf. Num. Ship Hydrodynamics, Gaithersburg, ML, Oct. 20-23, 1975

[31] S. Osher and R.P. Fedkiw, Level Set Methods: An Overview and Some Recent Results, J. Comput. Phys. 169 (2001) 463-502.

[32] S. Osher, and R.P. Fedkiw, Level Set Methods and Dynamic Implicit Surfaces, Springer-Verlag, (2002)

[33] S.J. Osher and J.A. Sethian, Fronts propagating with curvature dependent speed: algorithms based on Hamilton-Jacobi formulations, J. Comput. Phys. 79 (1988) 12-49.

[34] C.S. Peskin, The immersed boundary method, Acta Numerica (2002) 1-39.

[35] C. S. Peskin and D. M. McQueen, Modeling prosthetic heart valves for numerical analysis of blood flow in the heart, J. Comput. Phys. 37 (1980) 113-132.

[36] C. Pozrikidis, Interfacial dynamics for Stokes flow, J. Comput. Phys. 169 (2001) 250-301.

[37] E.G. Puckett, A.S. Almgren, J.B. Bell, D.L. Marcus, and W.J. Rider, A high-order projection method for tracking fluid interfaces in variable density incompressible flows, J. Comput. Phys. 130 (1997) 269-282.

[38] D.A. Porter and K.E. Easterling, Phase Transformations in Metals and Alloys, van Nostrand Reinhold, 1993.

[39] L. Rosenhead, The Formation of Vortices from a Surface of Discontinuity, Proc. R. Soc. Lond. A 134 (1932) 170-192.

[40] Lord Rayleigh, On the instability of jets, Proc. London Math. Soc. 10 (1879) 4-13.

[41] R.D. Richtmyer and K.W. Morton, Difference Methods for Initial-Value Problems, Inter-science, New York, 1967.

[42] Y. Renardy and M. Renardy, PROST: a parabolic reconstruction of surface tension for the Volume of Fluid method, J. Comput. Phys. 183 (2002) 400-421.

[43] Y.Y. Renardy, M. Renardy, V. Cristini, A new volume-of-fluid formulation for surfactants and simulations of drop deformation under shear at a low viscosity ratio, Eur. J. Mech. B 21 (2002) 49-59.

[44] J.A. Sethian, Level-Set Methods and Fast Marching Methods: Evolving Interfaces in Computational Geometry, Fluid Mechanics, Computer Vision and Materials Science, Cambridge University Press, Cambridge, MA (1999).

[45] M. Sussman, A.S. Almgren, J.B. Bell, P. Colella, L.H. Howell, and M.L. Welcome, An adaptive level set approach for incompressible two-phase flows, J. Comput. Phys. 148 (1999) 81-124.

[46] M. Sussman, A second order coupled level-set and volume-of-fluid method for computing growth and collapse of vapor bubbles. J. Comp. Phys. 187 (2003) 110-136.

[47] S. Shin and D. Juric, Modeling three-dimensional multiphase flow using a level contour reconstruction method for front tracking without connectivity, J. Comput. Phys. 180 (2002) 427-470.

[48] M. Sussman and G.E. Puckett, A coupled level set and volume-of-fluid method for computing 3D and axisymmetric incompressible two-phase flows, J. Comput. Phys. 162 (2000) 301-337.

[49] M. Sussman, P. Smereka, and S. Osher, A level set approach for computing solutions to incompressible two-phase flow, J. Comput. Phys. 114 (1994) 146-159.

[50] J. A. Sethian and P. Smereka, Level set methods for fluid interfaces, Annu. Rev. Fluid Mech. 35 (2003) 341-372.

[51] R. Scardovelli and S. Zaleski, Direct numerical simulation of free-surface and interfacial flow, Annu. Rev. Fluid Mech. 31 (1999) 567-603.

[52] G. Tryggvason, B. Bunner, A. Esmaeeli, D. Juric, N. Al-Rawahi, W. Tauber, J. Han, S. Nas, and Y.-J. Jan, A front-tracking method for the computations of multiphase Flow, J. Comput. Phys. 169 (2001) 708-759.

[53] A.K. Tornberg and Björn Engquist, Numerical approximations of singular source terms in differential equations, J. Comput. Phys. 200 (2004) 462-488.

[54] S.O. Unverdi and G. Tryggvason, A front-tracking method for viscous, incompressible, multi-fluid flows, J. Comput. Phys. 100 (1992) 25-37.

[55] H.-C. Wu, W.-S. Hwang, and H.-J. Lin, Development of a three-dimensional simulation system for micro-inkjet and its experimental verification, Mater. Sci. Eng. A 373 (2004) 268-278.

[56] X. Zheng, A. Anderson, J. Lowengrub, and V. Cristini, Adaptive unstructured volume remeshing: Application to level-set simulations of multiphase flow, J. Comp. Phys., in review.

[57] P. Yue, J.J. Feng, C. Liu, and J. Shen, A diffuse-interface method for simulating two-phase flows of complex fluids, J. Fluid Mech. 515 (2004) 293-317.
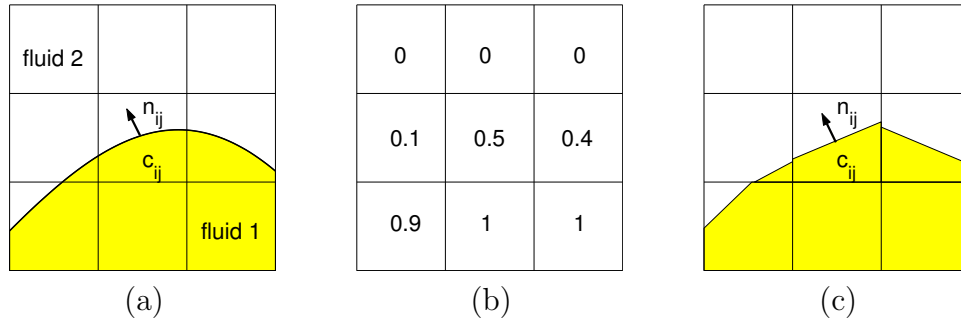
Figure 1: Volume-of-fluid representation of an interface: (a) actual interface, (b) volume fraction, and (c) an approximation to the interface is produced using an interface reconstruction method such as piecewise linear approximation as shown.
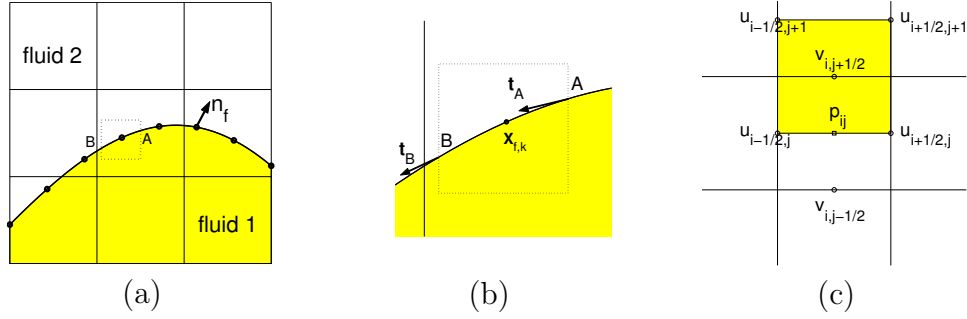
Figure 2: (a) The basic idea in the front tracking method is to use two grids - a stationary finite difference mesh and a moving Lagrangian mesh, which is used to track the interface. (b). Blow-up of the sub-grid control volume in (a); (c) Control volume for the Eulerian mesh, $\Omega_{i,j+\frac{1}{2}}$.
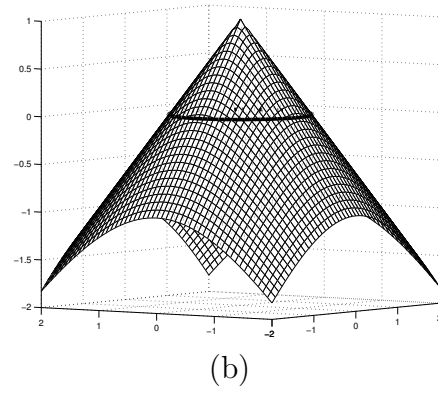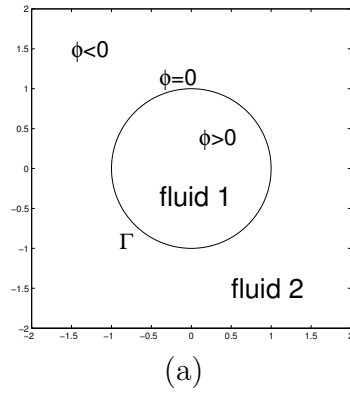
Figure 3: (a) Zero contour of ϕ representing the interface Γ. (b) Surface of ϕ with zero contour.
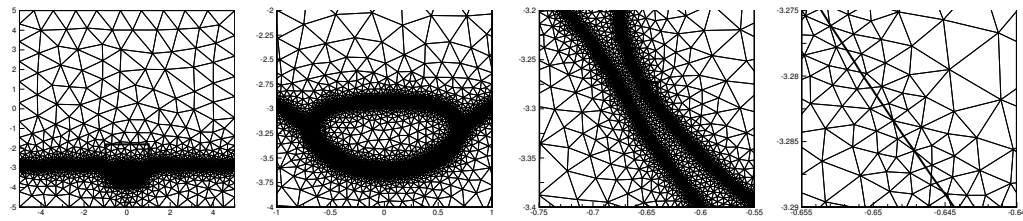
Figure 4: These figures are taken from X. Zheng, A. Anderson, J.S. Lowengrub and V. Cristini (unpublished), in which these meshes are used to simulate the drop-impacting interface problem. Each of the first three figures has a boxed region that is magnified in the next figure. The rates of magnification are 5, 10, 40/3, respectively.
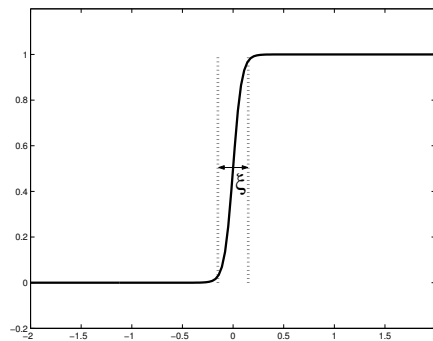
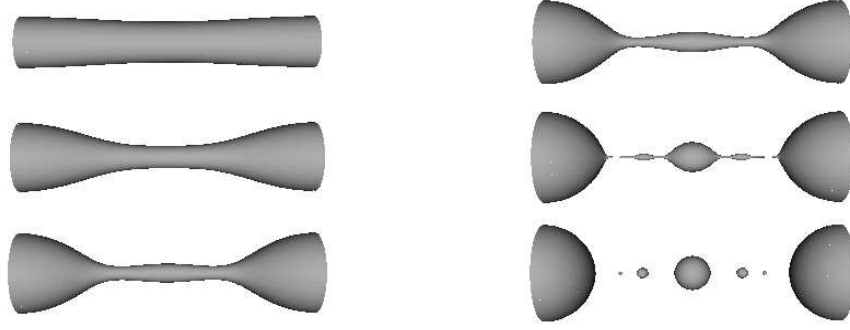Figure 5: A concentration profile across an interface with interface thickness, ξ.

Figure 6: Time evolution leading to multiple pinch-offs. The evolution is from top to bottom and left to right. The domain is axisymmetric, the initial velocities are zero everywhere, and the concentration field is given by $c(r, z) = 0.5 \left[1 - \tanh \left((r - 0.5 - 0.05 \cos(z))/(2\sqrt{2}\epsilon) \right) \right]$ on $\Omega = (0, \pi) \times (0, 2\pi)$. Densities are matched and viscosity ratio is 0.5.
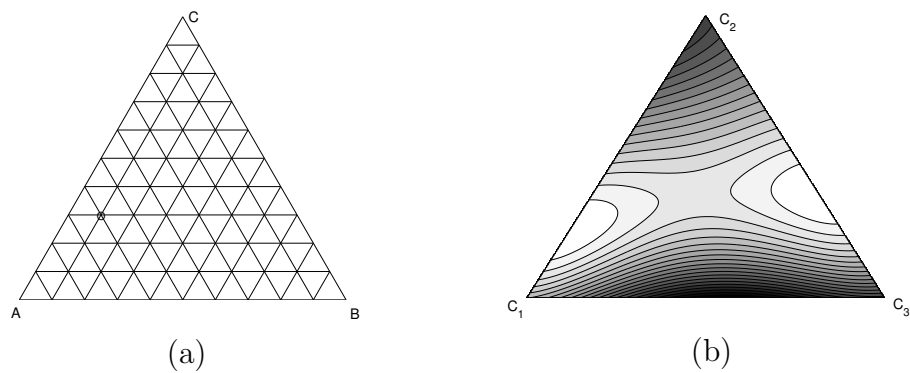
(a)

(b)

Figure 7: (a) Gibbs triangle. (b) Contour plot of the free energy $F(c_1, c_2)$ on the Gibbs triangle.
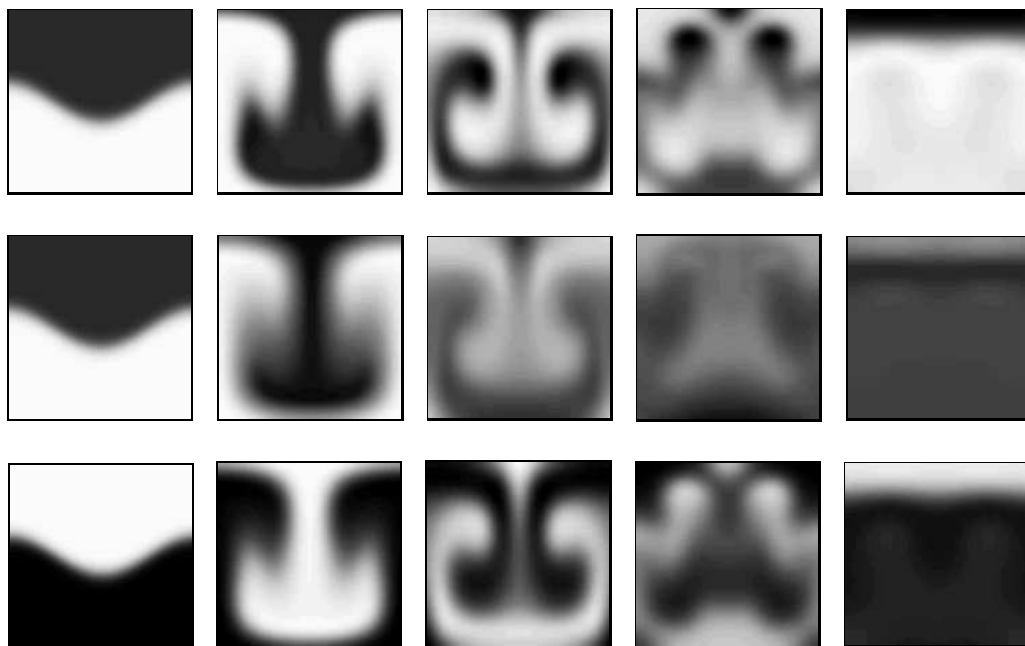
Figure 8: Evolution of concentration of fluid 1 (top row), 2 (middle row), and 3 (bottom row). The contours of c_1, c_2, and c_3 are visualized in gray-scale where darker regions denote larger values of c_1, c_2, and c_3, respectively.